The Open-Ring Line: A Low-Loss Surface Waveguide

CLAUDE FRAY AND ALBERT PAPIERNIK

Abstract—**This paper presents the theoretical analysis of the electromagnetic properties of the open-ring line by means of the Hankel transform. Fields components, stored energy, power flow, dispersion relation, and energy distribution are calculated. Measurements have corroborated our theoretical results. These results help in the design of low-loss line operating in the fundamental dipolar hybrid mode. The measured attenuation on a prototype line consisting of equally spaced aluminum rings held by a metal rod is less than 5 dB/km below 1.8 GHz. Among the possible applications are railway traffic control and railway obstacle detection.**

I. Introduction

COMPREHENSIVE reviews of low-loss open transmission lines were recently given [1]–[4]. Such lines have possible practical applications such as railway traffic control, railway obstacle detection, and telecommunications. Low-loss open guides may be divided into leaky waveguides such as the TE_{01} mode leaky circular waveguide [5] and surface waveguides such as the Goubau line [6] or the corrugated Y guide [7]. The open-ring line consisting of equally spaced metallic rings is a surface waveguide. We have investigated this periodic structure because of its theoretical importance and because of its expected low-loss characteristics. Preliminary theoretical results have been presented at the 1976 MTT-S International Symposium [8].

An exact approach consists of matching the field components inside and outside the ring line. In that way, we obtain a homogeneous system of linear equations. The dispersion relation follows from the requirement that the determinant vanishes. This procedure is burdensome because a determinant of large dimension must be solved to achieve sufficient accuracy. We shall assume that the rings are infinitely thin, are perfectly conducting, and have a width small compared with the line pitch and the wavelength (Fig. 1). Postulating a likely current distribution on the rings and using the Hankel transform of the fields, we deduce the field components, the stored energy, and the power flow. The dispersion relation is obtained either by equating the magnetic and electric stored energies or else by writing the boundary condition on the rings. Measurements have corroborated the calculated values. These results permit the design of low-loss rings line operating in the fundamental dipolar mode.

Manuscript received December 15, 1977; revised April 3, 1978.

The authors are with the U.E.R. des Sciences, Laboratoire d'Electronique des Microondes Equipe de Recherche Associée au C.N.R.S., Université de Limoges, 87060 Limoges Cedex, France.

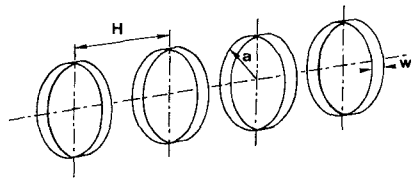

Fig. 1. Schematic representation of the open-ring line (a ring radius, H line period, w ring width).

II. Theoretical Formulation

A. Surface Current Density

Because the width w of the rings (Fig. 1) is small compared with the line pitch H, it is permissible to neglect the longitudinal (z-directed) current. Thus the field is produced only by the aximuthal current density J_θ

$$J_\theta = j_\theta \cos n\theta e^{j\omega t} = A\delta(r-a)e^{j(\omega t-\beta z)} \sum_{p=-\infty}^{\infty} f_p(z) \quad (1)$$

where A is a constant which determines current and field intensity, n is a positive integer which characterizes the symmetry in θ of the currents and fields, βH the phase shift between adjacent rings, and $f_p(z)e^{-j\beta z}$ the current distribution across the pth ring. We shall postulate for the current distribution that is applicable to an isolated narrow thin ring

$$f_p(z) = \left| w\left\{\left(z+\frac{w}{2}-pH\right)\left(pH+\frac{w}{2}-z\right)\right\}\right|^{-1/2}, \quad |z-pH| < \frac{w}{2}$$
$$0, \quad \text{elsewhere.} \quad (2)$$

This approximation was used earlier by Sensiper in his helical line study [9]. The variation in $\cos n\theta$ for the current density implies for the azimuthal variation of the fields components, through Maxwell's equations

$$E_r = e_r(r,z)\sin n\theta e^{j\omega t}, \quad E_\theta = e_\theta(r,z)\cos n\theta e^{j\omega t}$$
$$E_z = e_z(r,z)\sin n\theta e^{j\omega t}, \quad H_r = h_r(r,z)\cos n\theta e^{j\omega t}$$
$$H_\theta = h_\theta(r,z)\sin n\theta e^{j\omega t}, \quad H_z = h_r(r,z)\cos n\theta e^{j\omega t}. \quad (3)$$

B. Field Component Expressions

From Maxwell's equations, we deduced the following relations satisfied by the longitudinal components:

0018-9480/78/1100-0886$00.75 ©1978 IEEE

$$\frac{\partial^2 e_z}{\partial r^2}+\frac{1}{r}\frac{\partial e_z}{\partial r}-\frac{n^2}{r^2}e_z+\frac{\partial^2 e_z}{\partial z^2}+k^2 e_z=-\frac{jn}{\omega\epsilon r}\frac{\partial j_\theta}{\partial z}$$

$$\frac{\partial^2 h_z}{\partial r^2}+\frac{1}{r}\frac{\partial h_z}{\partial r}-\frac{n^2}{r^2}h_z+\frac{\partial^2 h_z}{\partial z^2}+k^2 h_z=-\frac{1}{r}\frac{\partial(rj_\theta)}{\partial r} \quad (4)$$

where $k=\omega(\epsilon\mu)^{1/2}=\omega/c$ is the wavenumber, ϵ the permittivity, μ the permeability of the medium, and c the light velocity.

Using Hankel transform (see Appendix I), we obtain

$$\frac{\partial^2 e_z^{\{n\}}}{\partial z^2}+(k^2-s^2)e_z^{\{n\}}=-\frac{jn}{\omega\epsilon}\frac{\partial}{\partial z}\int_0^\infty J_n(rs)j_\theta\,dr$$

$$\frac{\partial^2 h_z^{\{n\}}}{\partial z^2}+(k^2-s^2)h_z^{\{n\}}=s\int_0^\infty rJ_n'(rs)j_\theta\,dr. \quad (5)$$

In the current density expression (1), the periodic function $\Sigma_p f_p(z)$ given by (2) is expanded in a Fourier series

$$j_\theta=A\delta(r-a)e^{-j\beta z}\sum_{p=-\infty}^{\infty}f_p(z)=\frac{I}{H}\delta(r-a)\cdot\sum_{m=-\infty}^{\infty}D_m e^{-j\beta_m z} \quad (6)$$

where $I=aw$ is the total current on a ring, and

$$D_m=\frac{1}{\pi}\int_{-H/2}^{+H/2}\frac{e^{2\pi jmz/H}}{\sqrt{\left(z+\frac{w}{2}\right)\left(\frac{w}{2}-z\right)}}\,dz=J_0\left(m\pi\frac{w}{H}\right)$$

$$\beta_m=\beta+2m\pi/H.$$

Thus we have

$$e_z^{\{n\}}=\frac{nI}{\omega\epsilon H}\sum_{m=-\infty}^{\infty}\beta_m D_m e^{-j\beta_m z}\frac{J_n(as)}{s^2+\alpha_m^2}$$

$$h_z^{\{n\}}=-\frac{Ia}{H}\sum_{m=-\infty}^{\infty}D_m e^{-j\beta_m z}\frac{sJ_n'(as)}{s^2+\alpha_m^2} \quad (7)$$

with

$$\alpha_m^2=\beta_m^2-k^2.$$

Introducing the magnetic transverse component into the relation $\nabla\cdot\boldsymbol{H}=0$ and the z component of $\nabla\times\boldsymbol{H}=j\omega\epsilon\boldsymbol{E}$, we obtain

$$(h_r+h_\theta)^{\{n+1\}}=\frac{1}{s}\left[j\omega\epsilon e_z^{\{n\}}-\frac{\partial h_z^{\{n\}}}{\partial z}\right]$$

$$(h_r-h_\theta)^{\{n-1\}}=\frac{1}{s}\left[j\omega\epsilon e_z^{\{n\}}+\frac{h_z^{\{n\}}}{\partial z}\right]. \quad (8)$$

Similarly, introducing the electric transverse component into the relation $\nabla\cdot\boldsymbol{E}=(\nabla\cdot\boldsymbol{J})/j\omega\epsilon$ and the z component of $\nabla\times\boldsymbol{E}=-j\omega\mu\boldsymbol{H}$, we obtain

$$(e_r-e_\theta)^{\{n+1\}}=\frac{1}{s}\left[j\omega\mu h_z^{\{n\}}-\frac{\partial e_z^{\{n\}}}{\partial z}-\frac{jn}{\omega\epsilon}\int_0^\infty J_n(rs)j_\theta\,ds\right]$$

$$(e_r+e_\theta)^{\{n-1\}}=\frac{1}{s}\left[j\omega\mu h_z^{\{n\}}+\frac{\partial e_z^{\{n\}}}{\partial z}+\frac{jn}{\omega\epsilon}\int_0^\infty J_n(rs)j_\theta\,ds\right]. \quad (9)$$

The fields components are obtained by means of the inverse Hankel transform (Appendix I) and using the following integral [10]:

$$F_{nm}(a,r)=\int_0^\infty s\frac{J_n(as)J_n(rs)\,ds}{s^2+\alpha_m^2}=\begin{cases}K_n(\alpha_m a)I_n(\alpha_m r), & r<a\\ I_n(\alpha_m a)K_n(\alpha_m r), & r>a\end{cases}. \quad (10)$$

We have ($e^{j\omega t}$ is omitted)

$$E_z=\frac{nI}{\omega\epsilon H}\sin n\theta\sum_{m=-\infty}^{\infty}\beta_m D_m F_{nm}e^{-j\beta_m z}$$

$$E_r=\frac{jnI}{\omega\epsilon H}\sin n\theta\sum_{m=-\infty}^{\infty}\frac{D_m}{\alpha_m^2}\left[\beta_m^2\frac{\partial F_{nm}}{\partial r}+\frac{k^2a}{r}\frac{\partial F_{nm}}{\partial a}\right]e^{-j\beta_m z}$$

$$E_\theta=\frac{jI}{H}\cos n\theta\sum_{m=-\infty}^{\infty}\frac{D_m}{\alpha_m^2}\left[\frac{n^2}{r}\beta_m^2F_{nm}+k^2a\frac{\partial^2F_{nm}}{\partial a\partial r}\right]e^{-j\beta_m z}$$

$$H_z=\frac{-Ia}{H}\cos n\theta\sum_{m=-\infty}^{\infty}D_m\frac{\partial F_{nm}}{\partial a}e^{-j\beta_m z}$$

$$H_r=\frac{-jI}{H}\cos n\theta\sum_{m=-\infty}^{\infty}\frac{D_m}{\alpha_m^2}\beta_m\left[\frac{n^2}{r}F_{nm}+a\frac{\partial^2F_{nm}}{\partial a\partial r}\right]e^{-j\beta_m z}$$

$$H_\theta=\frac{jnI}{H}\sin n\theta\sum_{m=-\infty}^{\infty}\frac{D_m}{\alpha_m^2}\beta_m\left[\frac{\partial F_{nm}}{\partial r}+\frac{a}{r}\frac{\partial F_{nm}}{\partial a}\right]e^{-j\beta_m z}. \quad (11)$$

It is useful to check that, at $r=a$, the tangential electric field is continuous everywhere

$$E_z^i=E_z^e,\quad E_\theta^i=E_\theta^e$$

and that the discontinuity in the tangential magnetic field is proportional to the total surface current density

$$H_z^i-H_z^e=\frac{I}{H}e^{j\omega t}\cos n\theta\sum_{m=-\infty}^{\infty}D_m e^{-j\beta_m z}.$$

The subscripts i and e refer, respectively, to the internal ($r<a$) and external ($r>a$) field. These relations verify the continuity requirement of the fields at $r=a$.

III. Energetic and Dispersion Relations

A. Stored Energy

After integration over θ, the time-average magnetic energy and the time-average electrical energy per unit length are

$$\overline{W}_M=\frac{\pi\mu}{4H}\int_0^\infty\int_{-H/2}^{H/2}(h_r h_r^*+h_\theta h_\theta^*+h_z h_z^*)r\,dr\,dz$$

$$\overline{W}_E=\frac{\pi\epsilon}{4H}\int_0^\infty\int_{-H/2}^{H/2}(e_r e_r^*+e_\theta e_\theta^*+e_z e_z^*)r\,dr\,dz. \quad (12)$$

When the total field components are written in terms of their space harmonics, the general term of the double summation for $m\neq p$ can be written in the form $g_{nm}(r)f_{np}^*(r)\exp\{j(p-m)2\pi z/H\}$. After integration over z from $-H/2$ to $H/2$, the cross terms vanish and the resulting expression is the sum of the energy stored by each space harmonic individually. After applying the Hankel transform, (12) become

TABLE I
DISPERSION RELATION, STORED ENERGY, AND POWER FLOW
(ARGUMENT OF MODIFIED BESSEL FUNCTION IS $\alpha_m a$)

Dispersion relation	$\sum_{m=-\infty}^{\infty} \left\{ n^2 \frac{\beta_m^2}{\alpha_m^2} I_n(\alpha_m a) K_n(\alpha_m a) + k^2 a^2 I_n'(\alpha_m a) K_n'(\alpha_m a) \right\} D_m^2 = 0$
$\bar{W}_E = \frac{\pi I^2}{4\omega^2 \epsilon H^2}$	$\sum_{m=-\infty}^{\infty} \left\{ \frac{k^2 a}{2\alpha_m} \left[\frac{n^2}{\alpha_m^2}(\beta_m^2 + k^2) + k^2 a^2 \right] \left[I_n' K_n + I_n K_n' \right] - \frac{n^2 \beta_m^2}{\alpha_m^4}(k^2 - \alpha_m^2) I_n K_n - \frac{k^4 a^2}{\alpha_m^2} I_n' K_n' \right\} D_m^2$
$\bar{W}_M = \frac{\pi I^2 k^2}{4\omega^2 \epsilon H^2}$	$\sum_{m=-\infty}^{\infty} \left\{ \frac{a}{2\alpha_m} \left[\frac{n^2}{\alpha_m^2}(\beta_m^2 + k^2) + k^2 a^2 \right] \left[I_n' K_n + I_n K_n' \right] - \frac{n^2 \beta_m^2}{\alpha_m^4} I_n K_n - \frac{\beta_m^2 a^2}{\alpha_m^2} I_n' K_n' \right\} D_m^2$
$P = \frac{\pi I^2}{2\omega \epsilon H^2}$	$\sum_{m=-\infty}^{\infty} \frac{\beta_m}{\alpha_m} \left\{ \frac{a}{2} \left[\frac{n^2}{\alpha_m^2}(\beta_m^2 + k^2) + k^2 a^2 \right] \left[I_n' K_n + I_n K_n' \right] - \frac{n^2 k^2}{\alpha_m^3} I_n K_n - \frac{k^2 a^2}{\alpha_m} I_n' K_n' \right\} D_m^2$

$$\bar{W}_M = \frac{\pi\mu}{4}\int_0^\infty s\, h_z^{\{n\}} h_z^{*\{n\}}\, ds + \frac{\pi\mu}{8}\int_0^\infty s\Big[(h_r + h_\theta)^{\{n+1\}} \cdot (h_r^* + h_\theta^*)^{\{n+1\}} + (h_r - h_\theta)^{\{n-1\}}(h_r^* - h_\theta^*)^{\{n-1\}}\Big]\, ds$$

$$\bar{W}_E = \frac{\pi\epsilon}{4}\int_0^\infty s\, e_z^{\{n\}} e_z^{*\{n\}}\, ds + \frac{\pi\epsilon}{8}\int_0^\infty s\Big[(e_r - e_\theta)^{\{n+1\}} \cdot (e_r^* - e_\theta^*)^{\{n+1\}} + (e_r + e_\theta)^{\{n-1\}}(e_r^* + e_\theta^*)^{\{n-1\}}\Big]\, ds.$$

Using (8) and (9) and introducing the values of $e_z^{\{n\}}$ and $h_z^{\{n\}}$ given in (7), we obtain

$$\bar{W}_E = \frac{\pi I^2}{4\omega^2\epsilon H^2}\sum_{m=-\infty}^{\infty} D_m^2 \cdot \int_0^\infty \frac{a^2(s^2+1)s^2 J_n'^2(as) + n^2\beta_m^2 J_n^2(as)}{s^2(s^2+\alpha_m^2)^2}\, s\, ds$$

$$\bar{W}_E = \frac{\pi I^2}{4\omega^2\epsilon H^2}\sum_{m=-\infty}^{\infty} D_m^2 \cdot \int_0^\infty \frac{n^2\{\beta_m^2 s^2 + (s^2-k^2)\}^2 J_n^2(as) + k^4 a^2 s^2 J_n'^2(as)}{s^2(s^2+\alpha_m^2)^2}\, s\, ds.$$

Using the integrals given by Appendix II we obtain the expressions in Table I. The total stored energy per unit of length is

$$\bar{W} = \bar{W}_M + \bar{W}_E = 2\bar{W}_M = 2\bar{W}_E. \tag{13}$$

B. Power Flow

The time-average energy flow along the line is the real part of the integral of the complex Poynting vector over a cross section. After integration over θ, we obtain

$$P_z = \frac{\pi}{2}\,\mathrm{Re}\left[\int_0^\infty (e_r h_\theta^* - e_\theta h_r^*) r\, dr\right]. \tag{14}$$

The general term of the double summation $m \neq p$ is a function of z. But since the total power flow cannot be a function of z, it is permissible to take the average value P of P_z, over one period. Using the Hankel transform, the time-average power flow can be written in the form

$$P = \frac{\pi}{4}\int_0^\infty \Big[(e_r - e_\theta)^{\{n+1\}}(h_r^* + h_\theta^*)^{\{n+1\}} - (e_r + e_\theta)^{\{n-1\}}(h_r^* - h_\theta^*)^{\{n-1\}}\Big] s\, ds.$$

With (7)–(9), the power flow becomes

$$P = \frac{\pi I^2}{2\omega\epsilon H^2}\sum_{m=-\infty}^{\infty} D_m^2 \cdot \int_0^\infty \frac{k^2 a^2 \beta_m s^2 J_n'^2(as) - n^2\beta_m^2(s^2-k^2)J_n^2(as)}{s^2(s^2+\alpha_m^2)^2}.$$

Integrals given in Appendix II provide the final expression for the power flow in Table I.

C. Dispersion Relation and Group Velocity

The dispersion relation is obtained by specifying that $\bar{W}_M = \bar{W}_E$ (see Table I). The same dispersion relation could be obtained by writing

$$\int_V \boldsymbol{E}\cdot\boldsymbol{J}^*\, dV = 0$$

because, from Maxwell's equations

$$\bar{W}_M - \bar{W}_E = \frac{j}{4\omega}\int_V \boldsymbol{E}\cdot\boldsymbol{J}^*\, dV = 0 \tag{15}$$

where V is the volume where the current is different from zero, that is, on the ring surface. The group velocity which, for a periodic structure, is equal to the energy velocity [11], is the ratio of the average power flow to average stored energy per unit length

$$v_g = \frac{d\omega}{d\beta} = \frac{P}{\bar{W}}. \tag{16}$$

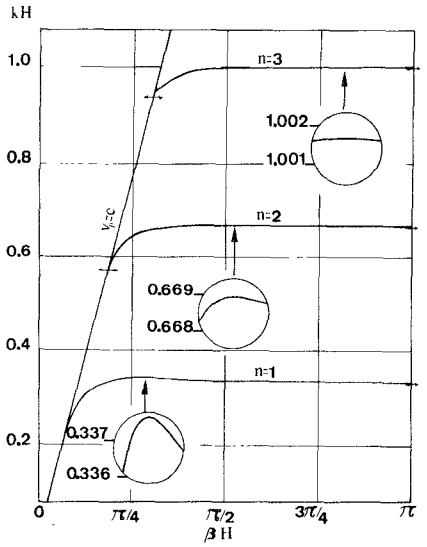

Fig. 2. Theoretical dispersion curves ($a/H=3$, $w/H=1/4$). The details of the curves near the maxima are shown inside the circles with an expanded vertical scale.

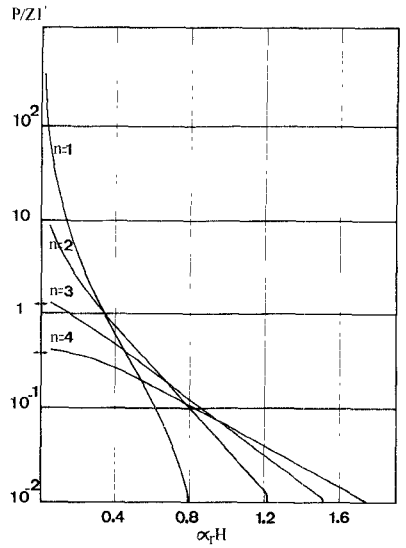

Fig. 3. Variation of the normalized power flow as a function of the radial propagation coefficient for the first modes ($a/H=3$, $w/H=1/4$).

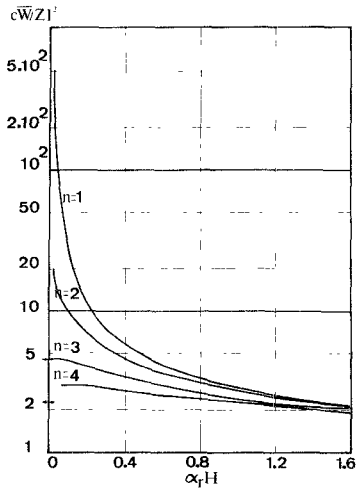

Fig. 4. Variation of the normalized stored energy as a function of the radial propagation coefficient for the first modes ($a/H=3$, $w/H=1/4$).

$\overline{W}$ is always positive and the group velocity has the same sign as the power flow. For $\beta H=\pi$ whatever the value of ω, P goes to zero because of pairing of equal positive and negative terms of the sum ($\beta_m=-\beta_{-m-1}$). This property is consistent with the requirement that the group velocity is zero at cutoff.

IV. Analysis of the Energetic and Dispersion Relations

The solution of the dispersion relation (Table I) gives the dispersion curves. But, to reduce the computation time, we have chosen to integrate (16), which can be written

$$\frac{dy}{dx}=f(x,y), \qquad \text{with } x=\beta H \quad \text{and} \quad y=kH.$$

This first-order differential equation is solved numerically using a fourth-order Runge–Kutta integration process with initial condition $y(x_0)=y_0$ obtained by solving the dispersion relation for $x_0=\pi$. The value of stored energy and of power flow is given during the integration process.

A particular line with $a/H=3$ and $w/H=1/4$ has been studied in detail. In the following figures, the limit values, obtained with only the fundamental term of the series reported in Table I, are represented by double arrows. Fig. 2 shows the dispersion curves of the three first modes. From this diagram, we see that only one hybrid wave can propagate along the line for each value of $n\neq 0$ and the circular symmetry mode $n=0$ does not exist. Accordingly, the fundamental mode has dipolar symmetry. For this value of a/H, the dispersion curves go through a maximum $(ka)_{\max}=n+\Delta n$ with $0<\Delta n\ll 1$; but when a/H decreases, the maximum goes on the right and disappears.

In Figs. 3 and 4, we have plotted the variation of power flow and stored energy for the first modes against the radial propagation coefficient $\alpha_r=(\beta^2-k^2)^{1/2}$. When α_r decreases to zero, $c\overline{W}/ZI^2$ and P/ZI^2 increase and tend to a limit for the modes 3 and 4, whereas they tend to infinity for the first two modes.

V. Comparison of Experimental and Theoretical Values

For recording the dispersion curves of the first modes, we introduced a section of the ring line between two metallic planes to obtain a resonator. The geometrical parameters of the line are equal to those of Fig. 5, but ring thickness is 0.5 mm. Two Teflon supports hold up the rings and keep constant the period.

From Fig. 5, we see that the experimental curves are practically identical to the theoretical ones (error is respectively less than 0.15 and 0.3 percent for the two first modes). The good agreement between the theoretical and experimental values of the π mode (Fig. 6) when the ring

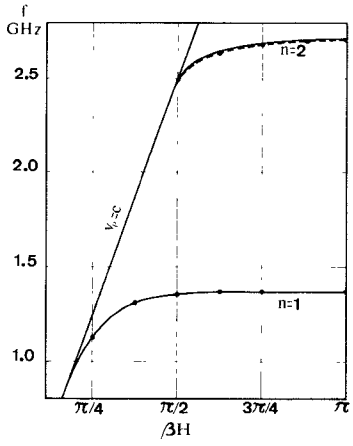

Fig. 5. Theoretical (———) and experimental (–·–·–·–) dispersion curves for the two first modes. Geometrical parameters: $2a=7.05$ cm, $H=3$ cm, $w=0.5$ cm ($a/H=1.175$, $w/H=1/6$).

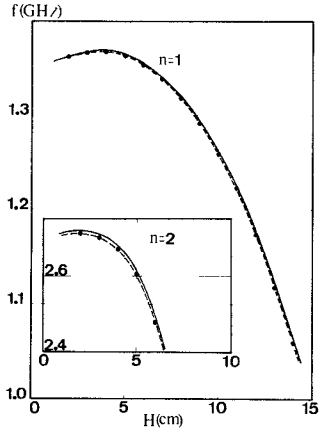

Fig. 6. Values of the π—cutoff versus period of the modes in Fig. 5 (———: theoretical, ·–·–·–: experimental).

pitch H increases, corroborates the validity of the theoretical analysis.

VI. Electromagnetic Energy Distribution Around the Line

The energy concentration around the line is measured by the amount of stored energy per unit length outside a cylinder of radius $d>a$ surrounding the line. This stored energy is given by (12) except for an integration over r from the radial distance d to infinity. Using the field components, we obtain, after rearranging, the following expression:

$$\overline{W}_{d\infty}=\frac{\pi I^2}{4\omega^2\epsilon H^2}\sum_{m=-\infty}^{\infty}D_m^2\left\{\left\{n^2\frac{\beta^2 m}{\alpha_m^2}I_n^2(\alpha_m a)+k^2a^2I_n'^2(\alpha_m a)\right\}\left\{k^2d^2\left\{K_n^2(\alpha_m d)\left(1+\frac{n^2}{\alpha_m^2d^2}\right)-K_n'^2(\alpha_m d)\right\}-\frac{\beta_m^2+k^2}{\alpha_m}dK_n'(\alpha_m d)K_n(\alpha_m d)\right\}-4n^2\frac{\beta_m^2k^2a}{\alpha_m^3}I_n(\alpha_m a)I_n'(\alpha_m a)K_n^2(\alpha_m d)\right\}.$$

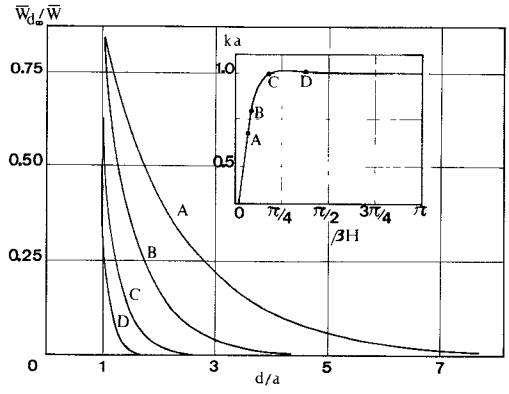

Fig. 7. Field extension around the ring line against the ratio d/a ($d\geq a$) with $a/H=3$, $w/H=1/4$.

The ratio of the stored energy outside a cylinder of radius d to the total stored energy ($\overline{W}_{d\infty}/\overline{W}$) for the dipolar mode, is plotted against d/a for various points of the dispersion curve in Fig. 7. The rapid decrease of the field extension with increasing $\alpha_r=(\beta^2-k^2)^{1/2}$ can be noticed. This property gives the possibility of restricting the field extension to any desired value.

VII. Study of a Low-Loss Prototype Line

The fundamental mode is somewhat different from the other modes of the ring line. Its dispersion curve goes down to low frequencies with a phase velocity and a group velocity near to the light velocity. The power flow becomes large, and the field extension around the line is important. Accordingly, the line attenuation $\alpha_z=P_J/2P$ (P_J ohmic losses and P power flow) tends to zero as P increases for I constant. So, by varying the phase constant β of this mode, it is possible to select the concentration of energy around the rings and the value of attenuation. Loss measurements have been made on a prototype line operating on this mode.

A. Prototype Line and Measuring Equipment.

The line consists of rings at equally spaced intervals along a metallic rod (Fig. 8). The electromagnetic influence of the rod is small because the mode is dipolar. The rings and the rod are of an aluminum alloy ($AGST_4$) for which the conductivity is $\sigma=2.857\times10^7$ ℧/m. A section of this structure is introduced between two aluminum plates, 2-m square, to form a resonator. One of these plates is fixed, the other attached to a movable carriage permitting adjustment of the resonator length. A series of holes was drilled in these short-circuit planes, allowing us to investigate the r and θ variation of the field [12].

B. Dispersion Curve and Attenuation Constant

Fig. 9 shows the theoretical (a) and experimental (b) dispersion curves of the dipolar mode. The slight discrepancy between theoretical and experimental values is explained by the fact that there is no rod in the theoretical case. On the other hand, the rod introduces another mode

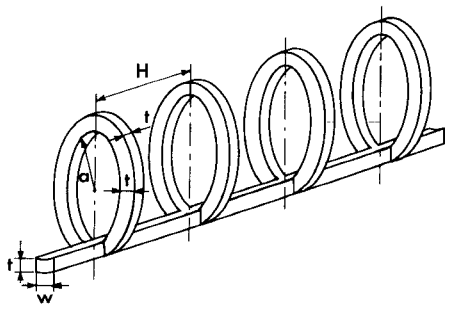

Fig. 8. Low-loss prototype line ($2a=0.03$ m, $H=0.028$ m, $w=t=0.005$ m).

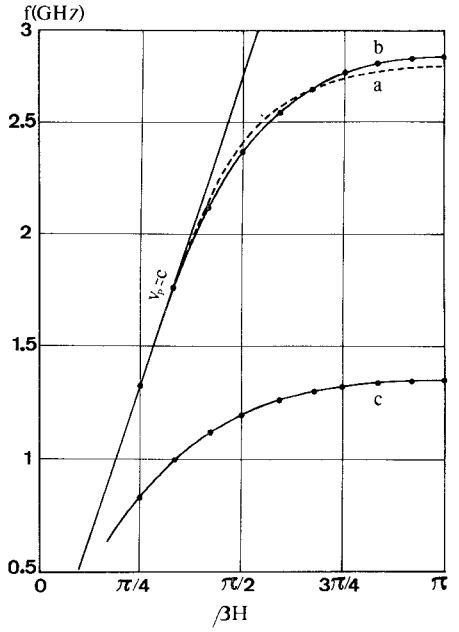

Fig. 9. Dispersion curves of the prototype line (Figs. 8, 9) a ——theoretical curve and b ·–·–·– experimental curve for the dipolar mode.

(c) but its stopband frequency is much lower than that in the dipolar mode. It corresponds to the fundamental mode of the structure studied by Birdsall and Everhart [13]. This periodic structure is a modification of the contrawound helix introduced by Chodorov and Chu [14]. Measured attenuation of this mode is important. The attenuation constant of the dipolar mode is obtained by the classical relation $\alpha_z=\omega/2v_gQ_0$ where Q_0 is the Qfactor of the line. To that effect, we measured the Qfactor of the resonator by transmission method for several lengths of the line at the same frequency; Q_0 is deduced from the Qfactor of the resonator by subtracting losses on the short-circuit planes [15]. Fig. 10 shows the relative phase velocity and the measured attenuation for the line shown in Fig. 8. The attenuation is less than 5 dB/km below 1.8 GHz. A theoretical estimation of attenuation has been made elsewhere, and these values corroborate the experimental ones [15]. Field distribution near the ring line was obtained [16] with close agreement between measured and calculated values, but we omitted it from this paper. For instance, the electromagnetic energy distribution is contained in a 40-cm ($=26.7$ a) radius cylinder when α_z is equal to 10 dB/km.

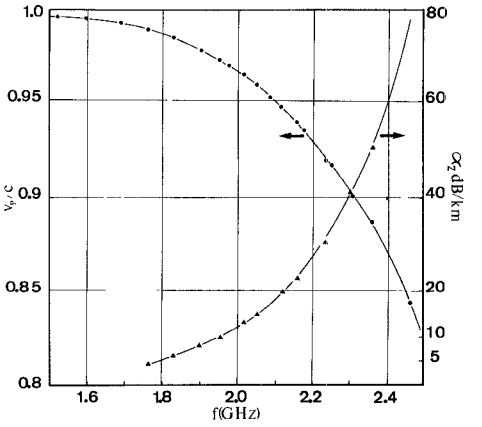

Fig. 10. Measured variation of the relative phase velocity and attenuation as a function of frequency.

VIII. Conclusions

The open-ring line is a surface waveguide just like dielectric rods and dielectric pipes. But its dispersion diagram is quite different because it does not have circularly symmetric TE or TM modes. However, the open-ring line and dielectric guides have one property in common: the fundamental mode is a hybrid dipolar mode without lower cutoff frequency. At lower frequencies, the electromagnetic wave propagates with phase velocity and group velocity near the light velocity, and the fields extend considerably beyond the line. By varying the radial propagation coefficient of this mode, it is possible to select the energy concentration around the rings and the power flow value. The wider the energy is spread, the smaller the attenuation constant. This property has been corroborated by the attenuation values of a prototype line operating on the dipolar mode of the ring line. The measured attenuation (less than 5 dB/km below 1.8 GHz) allows us to consider the open-ring line as a low-loss line. The line attenuation can be improved if the aluminum rings are replaced by copper rings. This line can be supported above the ground on plastic pipes that have to be set on the plane of rod. In this way, the electromagnetic field is only slightly perturbed (dipolar mode). These results show that practical applications like railway traffic control and railway obstacle detection may be considered [17]. In such applications, considerable difficulties may be encountered due to bends in the path of the line, scattering by the supports, and atmospheric conditions. Further studies could be required to analyze such effects.

Appendix I
Hankel Transform Properties [18], [19]

The n-order Hankel transformation transforms a function $u(r)$ into a new function $u^{\{n\}}(s)$ such that

$$u^{\{n\}}(s)=\int_0^\infty r\,J_n(rs)u(r)\,dr$$

$$u(r)=\int_0^\infty s\,J_n(rs)u^{\{n\}}(s)\,ds.$$

Operational properties

$$\left(\frac{u}{r}\right)^{\{n\}} = \frac{s}{2n}\left[u^{\{n+1\}} + u^{\{n-1\}}\right]$$

$$\left(\frac{du}{dr}\right)^{\{n\}} = -\frac{s}{2n}\left[(n+1)u^{\{n-1\}} - (n-1)u^{\{n+1\}}\right]$$

$$\left[\frac{1}{r}\frac{d(ru)}{dr}\right]^{\{n\}} = \frac{s}{2}\left[u^{\{n+1\}} - u^{\{n-1\}}\right]$$

$$\left[\frac{d^2u}{dr^2} + \frac{1}{r}\frac{du}{dr} - \frac{n^2}{r^2}u\right]^{\{n\}} = -s^2u^{\{n\}}$$

and integral product

$$\int_0^\infty s\, u^{\{n\}}(s)v^{\{n\}}(s)\, ds = \int_0^\infty ru(r)v(r)\, dr$$

are well suited for cylindrical coordinate system.

Appendix II

$$\int_0^\infty \frac{sJ_n^2(as)ds}{s^2+\alpha^2} = I_n(\alpha a)K_n(\alpha a)$$

$$\int_0^\infty \frac{s^2J_n'^2(as)ds}{s^2+\alpha^2} = \alpha^2 I_n'(\alpha a)K_n'(\alpha a)$$

$$\int_0^\infty \frac{J_n^2(as)ds}{(s^2+\alpha^2)^2} = \frac{a}{2\alpha}\left\{I_n'(\alpha a)K_n(\alpha a) + I_n(\alpha a)K_n'(\alpha a)\right\}$$

$$\int_0^\infty \frac{s^2J_n'^2(as)s\, ds}{(s^2+\alpha^2)^2} = -\frac{\alpha a}{2}\left\{I_n'(\alpha a)K_n(\alpha a) + I_n(\alpha a)K_n'(\alpha a)\right\}\left\{1+\frac{n^2}{\alpha^2a^2}\right\}$$

$$\int_0^\infty J_n^2(as)\frac{ds}{s} = \frac{1}{2n}$$

$$\int_0^\infty sJ_n'^2(as)ds = -\frac{n}{2a^2}.$$

References

[1] H. M. Barlow, "Millimeter waves and optical waves for long distance telecommunications by waveguide," in *Proc. Electromagnetic Wave Theory*. New York: Pergamon, 1965, pt. 1, pp. 389–397.

[2] J. C. Beal, J. Josiak, S. F. Mahmoud, and V. Rawat, "Continuous access of guided communications (C.A.G.C.) for ground transportation system," *Proc. IEEE*, vol. 61, no. 5, pp. 562–568, May 1973.

[3] F. Ries and C. L. Cuccia, "Status report communications in mass transit guided roadway systems," *Microwave System News*, pp. 24–42, Dec./Jan. 1975.

[4] T. Nakahara and N. Kurauchi, "Millimeter waveguides with applications to railroad communications, in *Advances in Microwaves*, vol. 4. London: Acad. Press, 1969, pp. 191–300.

[5] J. Amemiya, N. Kurita, K. Uematsu, T. Nakahara, and N. Kurauchi, "Leaky waveguide radar system," *Sumitomo Elec. Tech. Rev.*, no. 9, pp. 82–92, 1967.

[6] R. G. Fitzgerell, L. L. Haidle, and J. F. Partch, "A surface-wave transmission line for vehicular communication," Final Tech. Rept. for U.S. Dept. of Transportation, Office of High Speed, Inst. for Tele. Sciences, Boulder, CO, 1970.

[7] Y. Amemiya, N. Kurita, T. Nakahara, N. Kurauchi, and T. Nagao, "Surface wave radar system," *Sumitomo Elec. Tech. Rev.*, no. 3, Jan. 1964.

[8] C. Fray and A. Papiernik, "Theoretical analysis of open ring line," presented at the 1976 Int. Microwave Symp., Cherry-Hill, NJ, June 14–16, 1976.

[9] S. Sensiper, "Electromagnetic wave on helical conductors," MIT Res. Lab. Elect., Cambridge, MA, Rep. 194, May 1951.

[10] I. S. Gradshteyn and I. M. Ryzhik, *Table of Integral Series and Products*. New York and London: Academic Press, 1965, p. 679 formula no. 6.541.

[11] D. A. Watkins, *Topics in Electromagnetic Theory*. New York: Wiley, 1958.

[12] A. Papiernik and C. Fray, "Low-loss open transmission line: The open ring line," *Electron. Lett.*, vol. 11, no. 10, 1975.

[13] C. K. Birdsall and T. E. Everhart, "Modified contra-wound helix circuits for high-power traveling wave tubes," *IRE Trans. Electron. Devices*, pp. 190–204, Oct. 1956.

[14] M. Chodorov and E. L. Chu, "Cross-wound helices for traveling-wave tubes," *J. Appl. Phys.*, vol. 26, pp. 33–34, Jan. 1955.

[15] C. Fray and A. Papiernik, "Theoretical and experimental attenuation of the open ring line," presented at the 6th European Microwave Conf., Rome, Italy, Sept. 14–17, 1976.

[16] C. Fray, "Propriétés électromagnétiques de la ligne à anneaux ouverte ou blindée," Thesis, Université de Limoges, Limoges, France, May 1977.

[17] A.N.V.A.R. 74-24-274 (French Patent), "Ligne ouverte à très faibles pertes."

[18] G. N. Watson, *A Treatise on the Theory of Bessel Functions*. Cambridge, England: Cambridge Univ. Press, 1966, pp. 453–468.

[19] S. Colombo, *Les Transformations de Mellin et de Hankel*, CNRS, 1959.